

NEUROSYSTEMS

Structural and functional connectivity between the lateral posterior–pulvinar complex and primary visual cortex in the ferret

Chunxiu Yu,¹ Kristin K. Sellers,^{1,2} Susanne Radtke-Schuller,¹ Jinghao Lu,¹ Lei Xing,³ Vladimir Ghukasyan,³ Yuhui Li,¹ Yen-Yu I. Shih,^{2,4,5,6} Richard Murrow^{5,7} and Flavio Fröhlich^{1,2,3,4,5,8}

¹Department of Psychiatry, University of North Carolina at Chapel Hill, 115 Mason Farm Road, NRB 4109F, Chapel Hill, NC 27599, USA

²Neurobiology Curriculum, University of North Carolina at Chapel Hill, Chapel Hill, NC, USA

³Neuroscience Center, University of North Carolina at Chapel Hill, Chapel Hill, NC, USA

⁴Department of Biomedical Engineering, University of North Carolina at Chapel Hill, Chapel Hill, NC, USA

⁵Department of Neurology, University of North Carolina at Chapel Hill, Chapel Hill, NC, USA

⁶Biomedical Research Imaging Center, University of North Carolina at Chapel Hill, Chapel Hill, NC, USA

⁷Department of Neurosurgery, University of North Carolina at Chapel Hill, Chapel Hill, NC, USA

⁸Department of Cell Biology and Physiology, University of North Carolina at Chapel Hill, Chapel Hill, NC, USA

Keywords: lateral posterior nucleus, local field potential, multiunit activity, networks, oscillations, pulvinar

Edited by László Acsády

Received 7 August 2015, revised 15 October 2015, accepted 22 October 2015

Abstract

The role of higher-order thalamic structures in sensory processing remains poorly understood. Here, we used the ferret (*Mustela putorius furo*) as a novel model species for the study of the lateral posterior (LP)–pulvinar complex and its structural and functional connectivity with area 17 [primary visual cortex (V1)]. We found reciprocal anatomical connections between the lateral part of the LP nucleus of the LP–pulvinar complex (LPI) and V1. In order to investigate the role of this feedback loop between LPI and V1 in shaping network activity, we determined the functional interactions between LPI and the supragranular, granular and infragranular layers of V1 by recording multiunit activity and local field potentials. Coherence was strongest between LPI and the supragranular V1, with the most distinct peaks in the delta and alpha frequency bands. Inter-area interaction measured by spike-phase coupling identified the delta frequency band being dominated by the infragranular V1 and multiple frequency bands that were most pronounced in the supragranular V1. This inter-area coupling was differentially modulated by full-field synthetic and naturalistic visual stimulation. We also found that visual responses in LPI were distinct from those in V1 in terms of their reliability. Together, our data support a model of multiple communication channels between LPI and the layers of V1 that are enabled by oscillations in different frequency bands. This demonstration of anatomical and functional connectivity between LPI and V1 in ferrets provides a roadmap for studying the interaction dynamics during behaviour, and a template for identifying the activity dynamics of other thalamo-cortical feedback loops.

Introduction

Synchronization of activity across cortical areas represents a fundamental mechanism by which information is routed and processed during cognition and behaviour. For example, in attention-demanding tasks, synchronization in specific frequency bands relays relevant information between sensory and higher-order cortical areas (Buschman & Miller, 2007; Gregoriou *et al.*, 2009). Such long-range synchronization may result from direct cortico-cortical interactions, or may be orchestrated by subcortical structures that are

reciprocally connected with the relevant cortical areas. The pulvinar nucleus may represent such a subcortical hub, as it organizes cortical network activity in the alpha frequency band (8–12 Hz) in response to attentional demands in non-human primates (Saalmann *et al.*, 2012). Additionally, human neuroimaging data (Kastner *et al.*, 2004; Fischer & Whitney, 2012; Zhang *et al.*, 2013) and lesion reports from human patients (Arend *et al.*, 2008; Snow *et al.*, 2009; Rinne *et al.*, 2013) support a model in which the pulvinar nucleus is a key element of the neural substrate of attention and saliency processing. Together, these data suggest that the pulvinar nucleus may act as a hub in large-scale functional networks that process sensory information in primates. Such a hub could gate and

Correspondence: Flavio Fröhlich, ¹Department of Psychiatry, as above.

E-mail: flavio_frohlich@med.unc.edu

route sensory information to meet attentional demands by selectively synchronizing the brain areas required for processing of salient sensory input (Grieve *et al.*, 2000).

Reciprocal connectivity has been demonstrated between the pulvinar nucleus and primary visual cortex (V1) in the primate (Lund *et al.*, 1975; Benevento & Rezak, 1976; Ogren & Hendrickson, 1977; Jones, 2007; Kaas & Lyon, 2007; Marion *et al.*, 2013). However, very little is known about the functional role of this feedback loop. Interestingly, a recent study showed that inactivation of the lateral pulvinar nucleus, which projects to V1 in primates, abolished visual responses in the superficial layers of V1, suggesting an important role of the pulvinar projections in regulating V1 output (Purushothaman *et al.*, 2012). However, the interaction dynamics between the two areas have remained unknown. To fill this gap, we studied the structural and functional connectivity between the lateral posterior (LP)–pulvinar complex and area 17 (V1) in ferrets. It is of note that there remains a considerable neuroanatomical debate about homologies across species. In particular, the structure of the posterior thalamus in carnivores may not map one-to-one onto the primate thalamus (Chalupa, 1977). In ferrets, the LP–pulvinar complex is defined by comparison with the cat (Jones, 2007). Importantly, the lateral part of the LP nucleus of the LP–pulvinar complex (LPI) in the cat is the only subdivision of the LP–pulvinar complex that receives input from and sends projections to areas 17 and 18 (Berson & Graybiel, 1978; Updyke, 1981; Segraves & Rosenquist, 1982; Berson & Graybiel, 1983; Raczkowski & Rosenquist, 1983; Abramson & Chalupa, 1985), comparable to the striate-recipient zone of the primate inferior pulvinar nucleus. On the basis of these connectivity findings in the cat, LPI in carnivores resembles the primate pulvinar nucleus in terms of its connections with V1. However, no detailed study of the structure, connectivity or network dynamics of LPI in ferrets has been reported. Here, we performed histological staining, anatomical tracing and electrophysiological studies to delineate the structural and functional connectivity between LPI and V1 in the ferret.

Materials and methods

Surgery

Female ferrets (*Mustela putorius furo*, aged 16–20 weeks, 750–1000 g) were used for tracing studies ($n = 3$) and electrophysiological recordings in a single terminal procedure ($n = 8$). The surgical methods have been previously described in detail elsewhere (Sellers *et al.*, 2013). Briefly, anaesthesia was induced with an intramuscular injection of ketamine (30 mg/kg) and xylazine (1–2 mg/kg). The ferrets were then intubated, and anaesthesia was maintained with isoflurane administered through mechanical ventilation (0.5–1.25% isoflurane, 10–11 mL, 50 beats/min, 100% medical-grade oxygen). Xylazine (1.5 mg/kg/h) with 5% dextrose lactated Ringer's (4.25 mL/h) was continuously administered intravenously through the cephalic vein. For the survival tracer injection surgical procedures, no xylazine but a higher isoflurane concentration (1.5–2.5%) was used. General anaesthesia was maintained throughout surgery and the duration of recordings, as assessed by complete absence of a withdrawal response to toe pinch. Physiological signals were continuously monitored (electrocardiogram, partial oxygen saturation, end-tidal CO₂, and rectal body temperature). End-tidal CO₂ was between 30 mmHg and 50 mmHg (Kohn, 1997) for all ferrets, and the temperature was maintained between 38.0 °C and 39.0 °C with a water heating blanket. The eyes of the ferret were protected during surgery by the application of paralube.

Anatomical tracing

Three female ferrets were used for tracing studies. To determine the projections from V1 to LPI, anterograde tracer was injected into V1. One ferret was microinjected with 0.6 µL of AAV5–CaMKII–ArchT–GFP (7.5×10^{12} vg/mL) in two sites of V1 (8.5 mm and 9 mm lateral from the midline, and 3 mm anterior from lambda). To explore the layer-specific connections between V1 and LPI, two different strategies were used. In one ferret, AAV5–CaMKII–hChR2 (H134R)–mCherry (4.5×10^{12} vg/mL) was microinjected (0.3 µL) into LPI (13 mm anterior from lambda, and 3.8 mm lateral from the midline) for anterograde labelling of projections in V1. Another ferret was injected with 0.4 µL of Alexa 488-conjugated cholera toxin subunit B (CTB) (2.5 µg/µL CTB-488; Invitrogen) into LPI for retrograde labelling of projections in V1. All of the injections were performed with a 1-µL Hamilton syringe and an infusion rate of 0.1 µL/min. All viral constructs were packaged and titered by the UNC Vector Core Facility. Adequate pain relief and post-surgery monitoring were provided as described previously (Sellers *et al.*, 2013). Ferrets were humanely killed for histology 12 days after injection for CTB tracing, and 9 weeks (ArchT–GFP) and 11 weeks (hChR2–mCherry) after the procedure for viral injections. All procedures were approved by the University of North Carolina Chapel Hill Institutional Animal Care and Use Committee, and were in accordance with the guidelines set forth by the National Institutes of Health and the US Department of Agriculture.

Histology

Ferrets were humanely killed with an overdose of sodium pentobarbital, and transcardially perfused with 0.1 M phosphate-buffered saline followed by 4% paraformaldehyde in 0.1 M phosphate-buffered saline for subsequent histological verification of recording locations and histochemical characterization. Following perfusion, the brains were post-fixed for at least 2 days in 4% paraformaldehyde, and then transferred to 30% sucrose. The brains of the eight ferrets used for electrophysiological recordings were cut into 60-µm sections with a vibratome (Vibratome series 3000 plus) or cryostat (VT-1200; Leica Microsystems), and processed for cytochrome oxidase (CO) staining. The staining protocol for CO comprised a combination of previously published procedures (Wong-Riley, 1979; Wiser & Callaway, 1996). Brain shrinkage was estimated to be ~15%, on the basis of the distance measured on sections and the distance between lesions used during the experiment. Recording sites were reconstructed on the basis of known distances from lesion locations. For histological analysis of the LP–pulvinar complex, two ferret brains with six to eight alternating stains of neighbouring 50-µm-thick cryostat sections were analysed. Stains of these series were performed according to the following standard protocols: cell stain (Nissl), fibre stain [myelin silver impregnation (Gallyas, 1979)], CO stain (Wong-Riley, 1979), parvalbumin (anti-parvalbumin, rabbit, 1 : 2500; Swant PV28), vesicular glutamate transporter 2 (VGluT2) (anti-VGluT2, guinea pig, 1 : 2000; Millipore AB2251), and acetylcholinesterase (AChE) (Geneser-Jensen & Blackstad, 1971). Imaging was conducted with a Nikon Eclipse 80i widefield microscope. For the tracer injection experiments, the brains were sliced into 50-µm coronal sections and counterstained with 4',6-diamidino-2-phenylindole (DAPI) for cell labelling. Confocal images of the mounted brain sections were acquired with a laser scanning confocal microscope (LSM 780; Carl Zeiss) equipped with a $\times 10$ objective (EC Plan-Neofluar; numerical aperture, 0.30; Carl Zeiss), a $\times 20$ objective (Plan-Apochromat; numerical aperture, 0.8; Carl Zeiss), and

a $\times 40$ objective (Plan-Apochromat; numerical aperture, 1.4; Carl Zeiss). To determine the injection sites, sections were imaged at $\times 10$. Expression at the injection sites was determined at $\times 20$. To examine the labelled cell bodies or fibres in the projection sites, sections were imaged at $\times 40$.

Magnetic resonance imaging

To facilitate localization and provide a starting point for bridging histology findings with a future magnetic resonance atlas of the ferret, magnetic resonance imaging (MRI) of a single ferret brain was performed (Fig. S1). We used a 9.4-T Bruker BioSpec system with a BGA-9S gradient insert and a 35-mm quadrature volume coil (Bruker, Billerica, MA, USA). After perfusion with a solution of 10% formalin and Magnevist (Bayer Schering Pharma, Montville, NJ, USA) (20 : 1 ratio), the brain was placed in an aprotic solvent, i.e. perfluoropolyether (Fomblin Y04; Kurt J. Lesker Company, Clairton, PA, USA), and scanned according to a magnetic resonance protocol with a high-resolution T2-weighted RARE sequence with a spectral width of 60 kHz, repetition time/echo time of 2500/45 ms, a field of view of 2.8×1.92 cm, a slice thickness of 0.75 mm, a matrix of 560×384 , a RARE factor of 8, and averages of 100, resulting in a spatial resolution of $50 \times 50 \times 750$ μm .

Multi-site electrophysiology and visual stimulation

Surgery provided access to V1 and LPI for electrophysiological recordings. Following an initial midline incision of the scalp, soft tissue was retracted, and a craniotomy was drilled over the left V1 (3 mm anterior from lambda, and 9 mm lateral from the midline) and over the left LPI (13 mm anterior from lambda, and 3.8 mm lateral from the midline). Furosemide was administered to reduce the likelihood of swelling (1 mg/kg, intramuscular injection). The dura was removed at each craniotomy location, and the brain was covered with warm, 4% agar in physiological saline. A stainless steel head post was implanted with bone screws anterior to the LPI craniotomy.

Following the surgical procedure, the ferret was positioned in a head-frame for simultaneous electrophysiological recordings in V1 and LPI to record local field potentials (LFPs) and multiunit activity (MUA) during spontaneous and visually evoked activity. In V1, activity in all cortical layers was simultaneously recorded with acutely inserted linear silicon probes (32 channels, 50- μm contact site spacing along the *z*-axis; Neuronexus, Ann Arbor, MI, USA); neural activity in LPI was recorded with acutely inserted single metal electrodes (tungsten microelectrode; shank diameter, 250 μm ; impedance, 500 k Ω ; FHC, Bowdoin, ME, USA). The reference for the V1 electrode was located on the same shank (0.5 mm above the most superficial recording site), and was placed in agar in saline above the surface of the cortex. A silver chloride wire positioned between skull and soft tissue and held in place with 4% agar in saline was the reference for the LPI electrode. Each electrode was slowly advanced with a micromanipulator (Narishige, Tokyo, Japan). Separate recording depths for each penetration in LPI were spaced 300–400 μm apart. Probes in V1 were positioned such that superficial electrodes showed low-amplitude LFP signals, and deep electrodes showed high-amplitude LFP signals; the electrode for the LPI was advanced to ~ 6.5 mm ventral from the surface of the cortex after the dura was removed. At the conclusion of each penetration, one or two electrolytic lesions (400 μm apart in the *z*-plane) were induced by passing currents (5 μA , 10 s, unipolar) through the tips of the metal recording electrodes in LPI.

Signals from V1 were amplified with MPA8I head-stages with gain 10 (Multichannel Systems, Reutlingen, Germany), and then amplified with gain 500 (Model 3500; A-M Systems, Carlsborg, WA, USA). Signals from LPI were amplified with gain 1000 (Model 1800; A-M Systems). All signals were digitized at 20 kHz (Power 1401; Cambridge Electronic Design, Cambridge, UK), and digitally stored by the use of SPIKE2 software (Cambridge Electronic Design). Upon placement of the recording electrodes, the ferret was presented with visual stimulation displayed on a 52×29 -cm monitor with a refresh rate of 120 Hz (1920×1080 pixels, GD235HZ; Acer, New Taipei City, Taiwan) at a distance of 40 cm from the ferret, filling 60° of the visual field horizontally (azimuth) and 40° of the visual field vertically (elevation). Visual stimulation was controlled by the PSYCHOPHYSICS toolbox (Brainard, 1997) and a GeForce580 GPU (NVIDIA, Santa Clara, CA, USA). During electrophysiological recordings, full-field black and white (randomized) flashes were presented for 33 ms, with 967-ms intervals (300 trials each) in order to assess visually evoked potentials. A set of different artificial and naturalistic stimuli was presented to the ferret in order to measure the network dynamics of sensory processing; each trial consisted of 10 s of visual stimulation bracketed by 10 s of grey screen (at 50% contrast). Each stimulus was presented 10 times in randomized order. The stimuli included 10 checkerboard frozen noise stimuli presented for 1 s each (1-Hz noise; NOI) and a naturalistic stimulus from a nature video clip of foxes (FOX; Planet Earth, BBC, London, UK). For all stimuli, the timing of individual frames was confirmed by a photodiode covering a small, fully covered, flashing square in the corner of the monitor. In addition, electrophysiological signals were recorded from V1 and LPI in the absence of visual stimulation (typical duration, 10 min), when the ferret was in complete darkness (spontaneous activity). The eyes of the ferret were open during all recordings, and moistened with physiological saline prior to the start of each recording.

Electrophysiology data analysis

Of the 47 thalamic recording sites, two recording locations could not be accurately localized, nine did not respond to our visual stimulation paradigm, and eight were in the lateral geniculate nucleus (LGN) (Fig. 5; Fig. S2). These 19 sites were excluded from analysis, resulting in a dataset of LFPs and MUA from 28 sites in LPI to be analysed. Neurophysiological data were analysed with custom-written MATLAB (Mathworks, Natick, MA, USA) scripts. LFP data were extracted by low-pass filtering of the raw broadband signal with a cut-off frequency of 300 Hz. MUA was extracted by applying a threshold of minus four times of the standard deviation to the highpass-filtered neurophysiological data (filter cut-off, 300 Hz; fourth-order Butterworth). Visual responses were first determined from full-field black ('off') or white ('on') stimuli presented for 33 ms. Peri-stimulus time histograms (PSTHs) were determined by computing the average spiking response across trials, with a bin width of 5 ms. Peak amplitudes were determined as peak multiunit firing rate in the first 100 ms after stimulus onset minus 99% of the mean baseline firing rate (500 ms) before stimulus onset, averaged across trials. This threshold was chosen to avoid contamination of the response by outlier values in the baseline activity period. The time of the first spike was computed as the average time elapsed between stimulus onset and the first spike across all trials. Half-peak latency was computed as the time elapsed between the stimulus onset and the time point when the response reached 50% of its peak. Spike-count variance was calculated as the variance of the number of spikes occurring between 10 ms and 150 ms after stimu-

lus onset. The spike-count mean was determined from the same window. Temporal jitter was determined by calculating the standard deviation of the time of the first spike after stimulus onset. Supragranular (layers L1–L2/3), granular (L4) and infragranular (L5–L6) electrode sites were identified by determining the CSD from the full-field, white stimuli (Rappelsberger *et al.*, 1981; Pettersen *et al.*, 2008). The superficial aspect of the granular layer corresponded to the top of the initial sink elicited by visual stimulation. CSD profiles were spatially smoothed with a Hanning window (Ulbert *et al.*, 2001). Responses to 10 s of visual stimuli were determined by computing channel-averaged, trial-averaged PSTHs. Firing-rate responses were computed as the ratio of multiunit firing rate during the stimulus to the multiunit firing rate in the 10-s window ('rest') preceding the stimulus.

Spectral analysis was performed by convolving the LFP signals with a family of Morlet wavelets (0.5–40 Hz, step width of 0.5 Hz), and then averaging over time. Spectra are presented on a logarithmic scale. The relative strengths of the individual classic electroencephalography frequency bands (delta, 0.5–4 Hz; theta, 4–8 Hz; alpha, 8–12 Hz; beta, 12–30 Hz; gamma, 30–40 Hz) were computed by normalizing the mean power in each frequency band with the total power between 0.5 Hz and 40 Hz (Sellers *et al.*, 2013). Power correlations (Wang *et al.*, 2012) were determined by computing the correlation coefficient between the power in individual 5-s segments of continuous recordings, with averages across channels based on the CSD analysis to split the V1 data into supragranular, granular and infragranular layers. Magnitude square coherence was determined on the same 5-s windows, and averaged across windows for the spontaneous activity recorded in the dark. Coherence before (REST) and during (NOI and FOX) visual stimulation were calculated from the 10-s LFP windows before and during visual stimulation. Averages for cortical layers were calculated across channels as for the other analyses. Baseline correction of coherence was conducted by subtracting the coherence of the matched, trial-shuffled dataset. The phase preference of MUA was determined by extracting the instantaneous phase of the bandpass-filtered LFP by use of the Hilbert transformation (individually for each frequency band) and building the phase histograms for all detected multiunit spikes in the other brain area. Phase preference was computed as the Kullback–Leibler (KL) distance to a matched uniform distribution (Fröhlich & McCormick, 2010). These metrics were determined across all recording sessions to build accurate histograms; error bars are shown as bootstrapped 95% confidence intervals (CIs). Phase preferences before and during visual stimulation were calculated from 10-s windows. If not noted otherwise, results are presented as averages across electrode sites corresponding to supragranular, granular or infragranular layers in V1, and statistical analyses were performed on the group of trial-averaged individual recordings (electrode locations). Except when noted otherwise, all statistical tests were performed by the use of factorial ANOVA (ANOVA function in MATLAB), with *post hoc* paired testing if the corresponding main effect or the interaction was significant at $P < 0.05$. To control for multiple comparisons, pairwise *post hoc* tests were performed with Tukey's honestly significant different test with a $P < 0.05$ significance cut-off.

Results

Localization and anatomical connection

In order to delineate the LP–pulvinar complex in ferrets, we performed histological characterization of the area with classic histochemical and immunohistochemical stains. We found that the

LP–pulvinar complex in the ferret is roughly comparable to that of the cat (Fig. 1; representative examples of relevant stains). It is located within the dorsal thalamus, medial to the LGN, and dorsal to the medial geniculate nucleus, and extends in the rostrocaudal dimension ~4 mm from the rostral beginning of the ventrobasal complex to the caudal end of the LGN. A large LP nucleus dominates the complex. As judged from distinct differences in chemoarchitecture and cytoarchitecture, the LP nucleus of the ferret has several subdivisions. As in the cat (Jones, 2007), the most posterior part, i.e. LPI, is easy to delineate, as it stains intensely for CO but weakly for AChE. In the cat, the LP nucleus has three subdivisions, each with a specific connectivity pattern. LPI is the only subdivision of the LP–pulvinar complex that receives projections from area 17 (V1) and area 18 (Berson & Graybiel, 1978; Updyke, 1981; Segraves & Rosenquist, 1982; Berson & Graybiel, 1983; Raczkowski & Rosenquist, 1983). The connectivity of LPI with area 17 (V1) and area 18 is reciprocal in the cat. We therefore focused on this subdivision of the LP–pulvinar complex for our study of interaction dynamics between the LP–pulvinar complex and V1 in the ferret.

We investigated whether LPI of the ferret shows similar anatomical connections between LPI and area 17 (V1) by anatomical tracing. To establish whether V1 projects to LPI, we injected AAV5–CaMKII–ArchT–GFP into V1 (Fig. 2A) at the posterior pole of the hemisphere. This location is the same as our electrophysiological recording sites (Fig. 5C). We found densely labelled terminals in a patch of LPI (Fig. 2B and enlargement in Fig. 2C), and also a band of expression in the LGN. The connectivity pattern is in accord with findings in the cat (Abramson & Chalupa, 1985), and confirms our delineation of LPI.

To further investigate the layer-specific connections between these two areas, we examined projections from V1 to LPI by injecting the retrograde tracer CTB-488 into LPI (Fig. 3A and B). We found retrogradely labelled pyramidal cells in the infragranular layers V–VI of V1 (Fig. 3C–D). To determine the presence of layer-specific projections from LPI to V1, we injected the anterograde viral tracer AAV5–CaMKII–hChR2 (H134R)–mCherry into LPI (Fig. 4A and B), and examined the projections in V1 (Fig. 4C and D). We found that mCherry-labelled projections densely terminated in layer I of V1, with some termination in layer III/upper layer IV, but almost none in the infragranular layers. This projection pattern of LPI to areas 17 and 18 has been described for the cat by several authors [reviewed in Jones (2007)], and further confirms our delineation of LPI. To locate the LP–pulvinar complex of the ferret in the brain, we also performed a structural MRI scan (Fig. S1), as no stereotaxic ferret brain atlas is currently available.

Full-field visual responses

We simultaneously recorded LFPs and MUA from LPI and V1 in the absence of visual input (spontaneous activity in the dark) and during the presentation of visual stimuli in the anaesthetized ferret (Fig. 5A). We used a single metal electrode to record from LPI, and a multichannel silicon probe with 32 vertically aligned channels to simultaneously record from all cortical layers in V1. The exact locations of the recording sites were confirmed by electric lesions and subsequent histology (Figs 5B, C, and S2). The eyes of the ferrets were open during all recordings.

To characterize visual responses, we used full-field white ('on') and black ('off') flashes (in randomized order). In order to assess the depth of the multichannel silicon probe in V1, we used CSD analysis to locate the current sinks and sources generated by the visual response to full-field white flashes across the depth of the

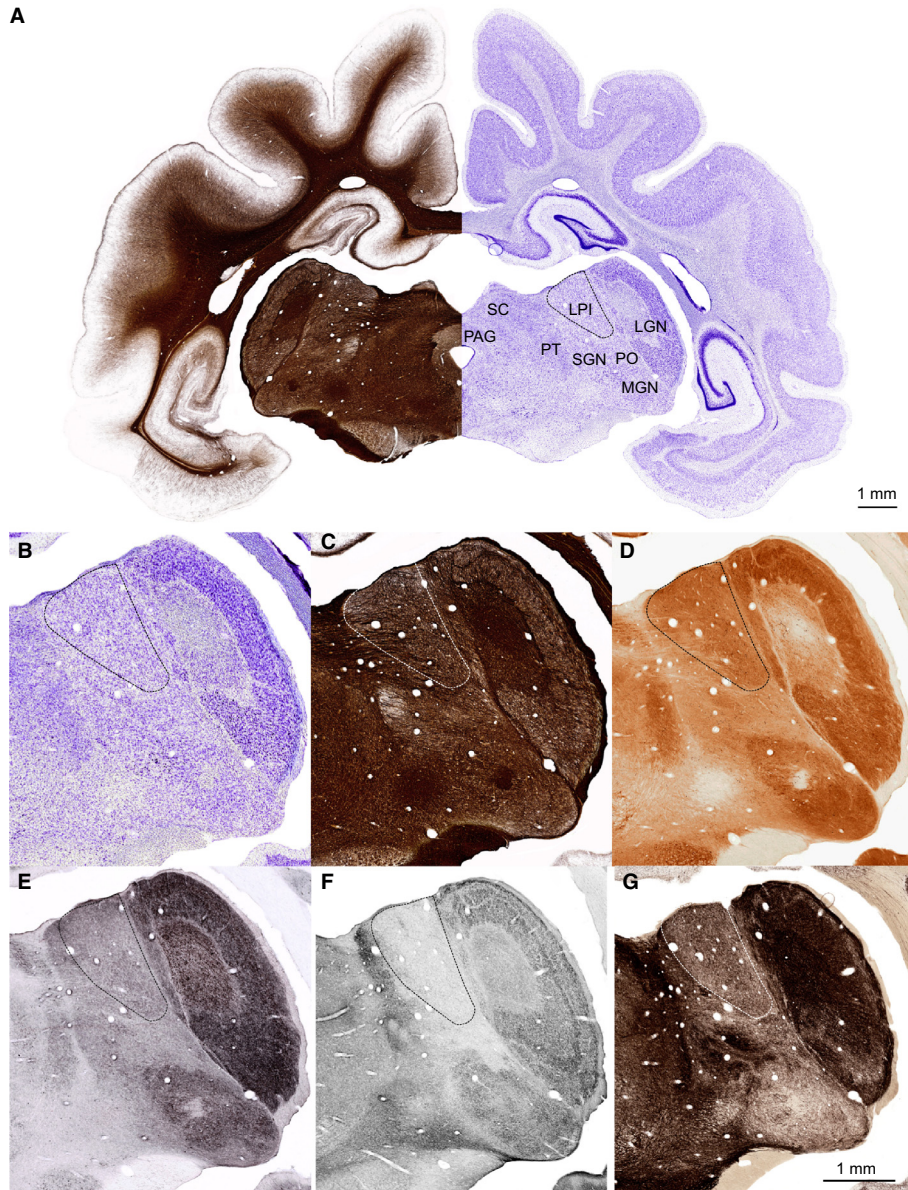


FIG. 1. Six stains of neighbouring 50- μm thick sections at the rostro-caudal level of the caudal LPI. (A) Composite image of a stained fibre (myelin silver impregnation) (Gallyas, 1979) and a mirrored neighbouring section stained for cells (Nissl). (B–G) Enlarged sections: (B) Nissl; (C) fibre; (D) CO; (E) parvalbumin; (F) VGluT2; (G) AChE. MGN, medial geniculate nucleus; PAG, periaqueductal grey; PO, nucleus of the posterior group; PT, pretectal nucleus; SC, superior colliculus; SGN, supragenulate nucleus.

cortex (Fig. 5D). The upper end of the superficial current sink was considered to be the point of alignment (superficial granular layer), and was used for averaging data across recordings.

Twenty-eight LPI recording locations (eight ferrets; examples in Fig. 5B, Fig. S2, and Table S1) showed responses to visual stimulation. MUA increased in response to the onset of the full-field white and black visual stimuli (Fig. 6A; population PSTHs). To quantify and compare the neuronal responses in LPI and V1 across layers (supragranular, LI–LII/III; granular, LIV; infragranular, LV/VI), we first determined the peak amplitude of MUA during ‘on’ and ‘off’ flashes (Fig. 6B, top). In LPI, MUA showed similar peak responses to both flashes ($P > 0.05$, rank-sum test). In contrast, a two-way ANOVA showed a significant main effect of stimulus type (‘on’ vs. ‘off’, $F_{1,727} = 244.65$, $P < 0.001$), a significant main effect of recording site (three V1 layers, $F_{2,727} = 13.8$, $P < 0.001$), but no

significant interaction between stimulus type and recording site ($F_{2,727} = 2.44$, $P > 0.05$) among the three V1 layers. According to *post hoc* comparisons, for ‘on’ flashes, the peak amplitude of MUA in the supragranular layers was significantly lower than in the granular and infragranular layers ($P < 0.05$). For ‘off’ flashes, the peak amplitude of MUA was not significantly different among V1 layers (supragranular, mean = 60.4 Hz; granular, mean = 90.5 Hz; infragranular, mean = 74.7 Hz; $P > 0.05$). We examined the timing of the first spike (measured from stimulus onset to the first spike) during ‘on’ and ‘off’ flashes (Fig. 6B, bottom). A two-way ANOVA with stimulus type (‘on’ or ‘off’) and recording site (LP–pulvinar complex; V1 cortical layers) as factors showed a significant main effect of recording site ($F_{3,1124} = 44.85$, $P < 0.001$), a main effect of stimulus type ($F_{1,1124} = 128.49$, $P < 0.001$), and a significant interaction between these factors ($F_{3,1124} = 3.31$, $P = 0.020$). *Post*

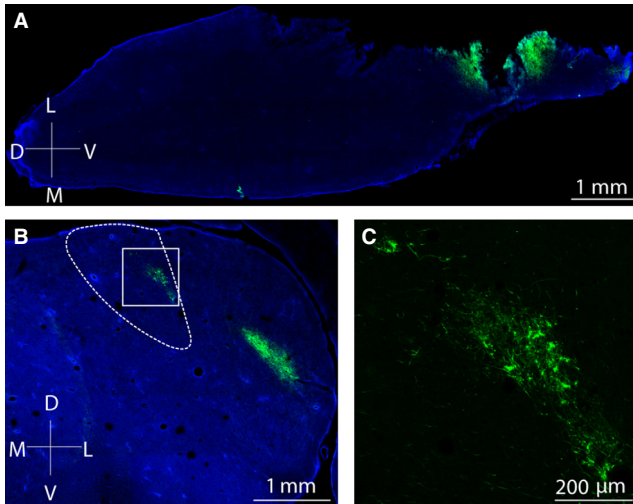


FIG. 2. Anterograde tracer injection shows that area 17 (V1) projects to LPI. (A) Focal injection site of rAA5–CaMKIIa–ArchT–GFP (green) in the most caudal part of area 17, which covers the whole cortical surface of the fore-brain hemisphere at that posterior level. (B) Restricted anterograde label in the caudal LPI (dashed outlined) and LGN. White square: location of C. (C) Labelled terminals in LPI. All sections were counterstained with DAPI.

hoc comparison showed that the time of the first spike in LPI MUA ('on', mean = 54 ms) was significantly later than those of V1 granular and infragranular MUA ($P < 0.05$; granular, 'on', mean = 30 ms; infragranular, 'on', mean = 31 ms) during 'on' flashes, but not significantly different from those of supragranular MUA (supragranular, 'on', mean = 47 ms). However, during 'off' flashes, the time of the first spike of LPI MUA ('off', mean = 65 ms) was statistically different from those of V1 granular neurons ('off', mean = 49 ms, $P < 0.05$), but not from those of supragranular and infragranular neurons (supragranular, 'off', mean = 68 ms; infragranular, 'off', mean = 60 ms). To confirm these findings, we also examined response latency measured from stimulus onset to half of the response peak during 'on' and 'off' flashes. A two-way ANOVA with stimulus type and recording site as

factors showed a significant main effect of recording site ($F_{3,774} = 23.18$, $P < 0.001$), no main effect of stimulus type ($F_{1,776} = 0.44$, $P = 0.51$), and a significant interaction between these factors ($F_{3,774} = 4.08$, $P = 0.007$). *Post hoc* comparison showed that the latencies of LPI MUA ('on', mean = 60 ms; 'off', mean = 51 ms) were significantly longer than those of V1 neurons ($P < 0.05$; supragranular, 'on', mean = 33 ms; supragranular, 'off', mean = 36 ms; granular, 'on', mean = 31 ms; granular, 'off', mean = 38 ms; infragranular, 'on', mean = 31 ms; infragranular, 'off', mean = 39 ms). This latter metric of onset delay measures a slightly different feature of the response, and may be more robust than the time of the first spike. Nevertheless, the overall picture was the same, in that V1 had shorter response latencies than LPI (with the potential exception of supragranular layers).

We next sought to further delineate the differences in visual processing between LPI and the different layers in V1; we assessed the variability of overall spike-count and of spike-timing. We measured spike-count variability to assess the trial-to-trial spike reliability by computing the mean and variance of the spike-count across 300 trials for each MUA recording for both 'on' and 'off' conditions (Fig. 6C). The variance scaled with the mean spike-count in V1 during both conditions (supragranular, 'on', slope = 0.80, 95% CI 0.78–0.83; supragranular, 'off', slope = 1.03, 95% CI 0.96–1.10; granular, 'on', slope = 0.67, 95% CI 0.62–0.72; granular, 'off', slope = 1.34, 95% CI 1.16–1.53; infragranular, 'on', slope = 0.74, 95% CI 0.61–0.87; infragranular, 'off', slope = 1.31, 95% CI 1.14–1.48). In contrast, the response in LPI showed higher variance as a function of the mean spike-count ('on', slope = 2.70, 95% CI 2.02–3.39; 'off', slope = 3.56, 95% CI 2.84–4.27). Thus, LPI responses to full-field visual stimuli were less reliable than V1 responses. We then examined the ability of LPI and V1 MUA to respond with high temporal precision from trial to trial by computing the jitter in the timing of the first spike after stimulus onset for both 'on' and 'off' stimuli (Fig. 6D). A two-way ANOVA showed a significant effect of stimulus type ($F_{1,1122} = 58.18$, $P < 0.001$) and a significant effect of recording site ($F_{3,1122} = 57.12$, $P < 0.001$). There was no significant interaction between these factors ($F_{3,1122} = 1.20$, $P = 0.28$). Thus, LPI MUA showed larger temporal variability than V1 neurons

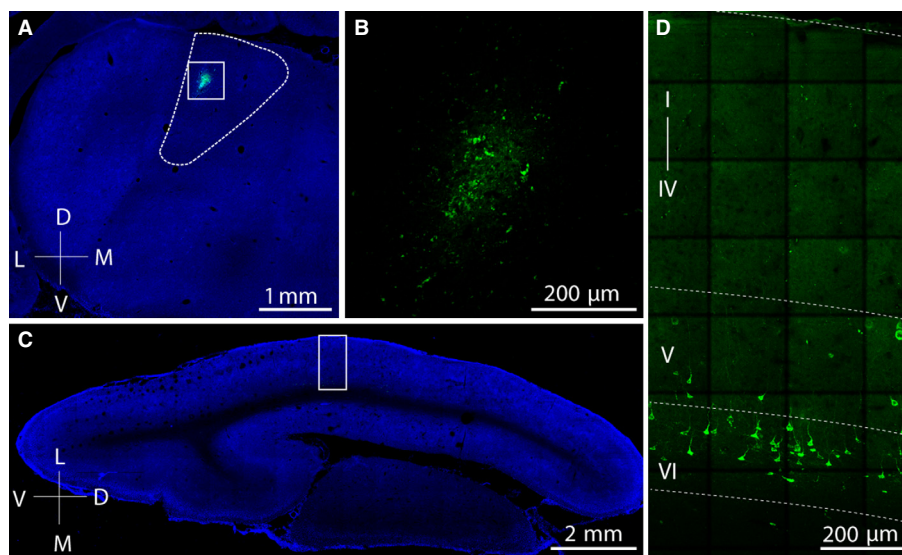


FIG. 3. Retrograde tracer injection established the layer-specific origin of fibres from area 17 (V1) that project to LPI. (A) Focal injection site of CTB-488 (green) in LPI. (B) Enlarged area from A (white square). (C) Retrograde labelling of pyramidal cells in layers V and VI are seen in the more anterior part of area 17. White square: location of the enlargement shown in D (confocal image). (D) CTB-488 label only. All sections were counterstained with DAPI. Dashed lines indicate the layer boundaries.

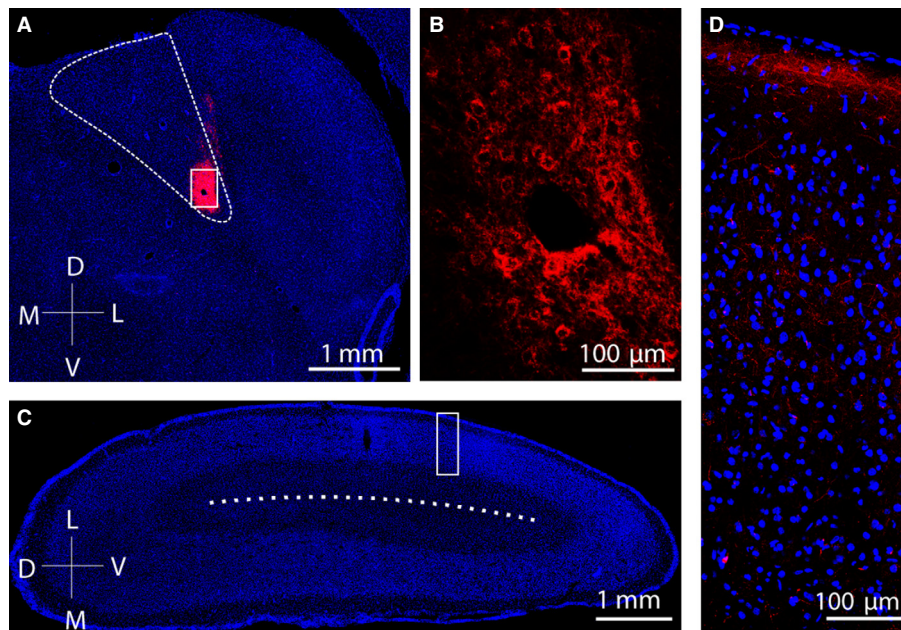


FIG. 4. Anterograde tracer injection delineated target layers of fibres from LPI in area 17 (V1). (A) Focal injection site of rAAV5–CaMKIIa–hChR2 (H134R)–mCherry (red) in the caudal LPI (outlined). White square: location of B. (B) Labelled cell bodies in LPI. (C) The most caudal part of V1, which covers the whole cortical surface of the forebrain hemisphere at that posterior level. The dashed line indicates the location of the almost non-existent underlying white matter at that posterior level. The white square marks the location of the enlargement in D. (D) Dense anterograde label in V1, predominantly in layer I, together with the DAPI-stained cell nuclei in a confocal image. All sections were counterstained with DAPI.

in both conditions ('on' jitter, mean = 35 ms; 'off' jitter, mean = 48 ms; $P < 0.05$). Meanwhile, supragranular neurons also showed significantly higher temporal jitter than granular and infragranular neurons ($P < 0.05$). Together, these data demonstrate that visual responses are, overall, less reliable in LPI than in V1, in agreement with the putative role of the LP–pulvinar complex as a higher-order thalamic structure. However, the similarity of LPI and the supragranular layers in V1 in terms of more pronounced jitter (in contrast to the more reliable granular and infragranular layers) may suggest closer interaction of LPI with the supragranular layers of V1.

Spontaneous oscillation dynamics of LFPs

We next analysed the mesoscale (LFP) interactions between LPI and V1, to elucidate the functional connectivity. We examined the LFP spectral compositions of the two areas individually, and assessed the correlation between them. In the absence of visual input (spontaneous activity), the power spectra of both LPI and V1 (all layers) showed pronounced power at low frequencies (<4 Hz, delta band), probably reflecting the fact that the recordings were performed under anaesthesia (Fig. 7A). In addition, the LFP recorded in LPI showed a clear spectral peak in the gamma frequency band (~30 Hz). The V1 LFPs (all three layers) did not show a gamma peak, but instead a modest spectral peak (~25 Hz) in the beta frequency band (12–30 Hz). To further probe these similarities and differences in frequency structure, we analysed the relative contributions of the different frequency bands to the overall power of the LFP signal (Fig. 7B) by computing the power in each frequency band as a percentage of total power. This normalization avoided potential confounds introduced by amplitude differences caused by different recording systems used in the two areas. Two-way ANOVA showed significant main effects of frequency band (delta, theta, alpha, beta, and gamma, $F_{4,500} = 1892.42$, $P < 0.001$) and no main effect of

recording site ($F_{3,500} = 0$, $P = 1.00$) for LFP spectral power. There was significant interaction between these factors ($F_{12,500} = 11.89$, $P < 0.001$). Pairwise comparisons confirmed the following findings from visual inspection of the spectra: (i) the largest contribution to the overall spectrum in both areas came from oscillations in the delta band ($P < 0.05$); (ii) the relative contributions of power in the delta and theta bands were significantly lower in LPI than in all three cortical layers ($P < 0.05$); and (iii) the relative gamma power in LPI was higher than that in all cortical layers ($P < 0.05$). The distribution of oscillatory power across frequency bands did not differ across V1 layers ($P > 0.05$).

Functional connectivity of LPI and V1 at the LFP level

To study the functional connectivity between LPI and V1 as a function of oscillatory activity, we applied the MRI resting state analysis strategy of assessing the correlations of spontaneous fluctuations of activity level measured by oscillation power as a function of frequency band (Wang *et al.*, 2012). Specifically, we investigated LFP power correlations between LPI and each V1 cortical layer by performing a correlation analysis of LFP spectral power at different frequency bands during spontaneous activity (i.e. dark, no visual input) (Fig. 7C and D). We divided the continuous recordings into 5-s segments, computed the correlation coefficients between the spectral powers, and averaged across channels corresponding to supragranular, granular or infragranular layers. We found a significant main effect of frequency band (two-way ANOVA, $F_{4,376} = 5.21$, $P < 0.001$), in which there were significantly higher correlations in alpha power between LPI and all three cortical layers than for delta, theta, beta, and gamma power (Fig. 7D). Although the power values in LPI and the supragranular layer showed higher alpha correlations, only trend-level differences were found between LPI and cortical layers ($F_{2,376} = 2.76$, $P = 0.07$). Also, no significant interaction was found between frequency band and different LPI–cortical

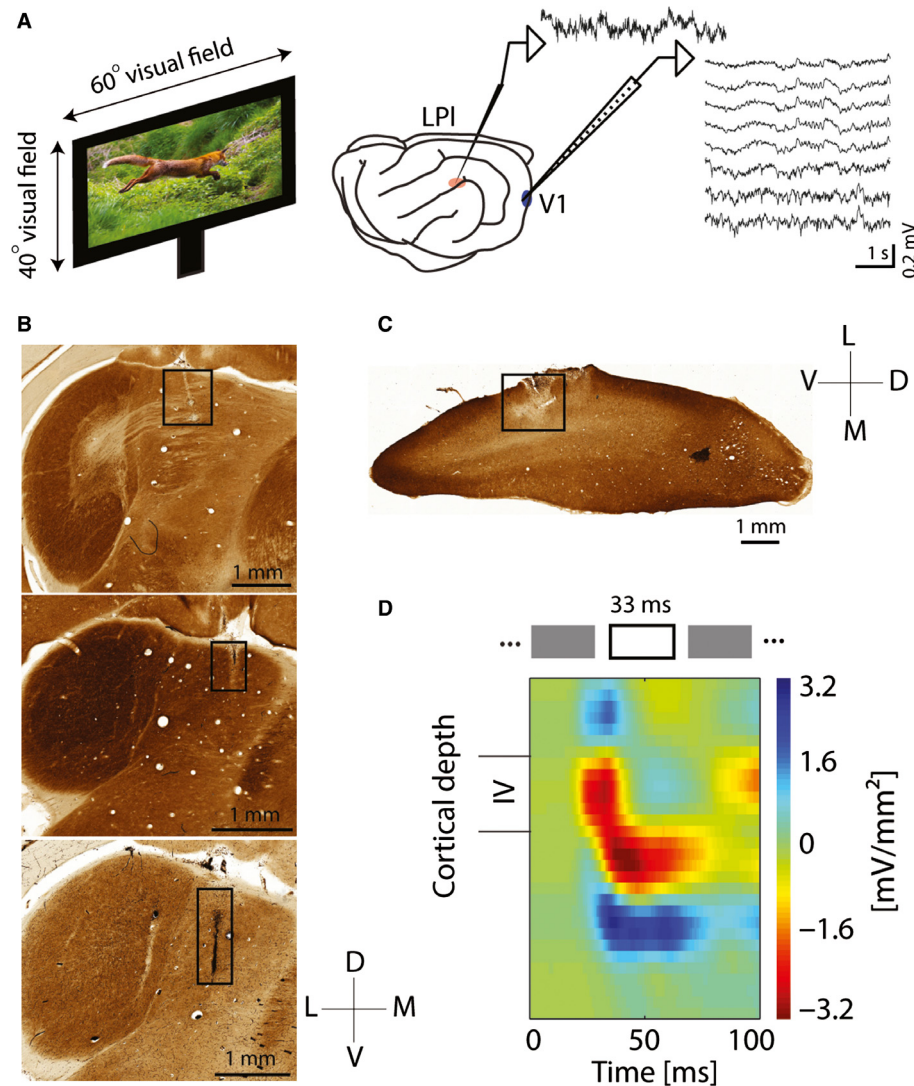


FIG. 5. Design of the electrophysiological recording study and identification of cortical layers. (A) Recording design. MUA and LFPs were recorded simultaneously from the left LPI (red) and the left V1 (blue) during spontaneous activity and visual stimulation. A single metal electrode was used in LPI, and a linear probe with 32 channels was used to simultaneously record from all cortical layers (sample raw LFP traces shown). The movie clip image shown is similar to original, copyright-protected movie clips from the BBC (Planet Earth). (B) Three CO-stained coronal sections with the electrode tracks and electrolytic lesions in the LPI (representative sections from three ferrets). (C) CO-stained coronal section with the track of the linear silicon probe in V1. (D) Top: stimulus design. Full-field white flashes were presented for 33 ms at a frequency of 1 Hz. Bottom: cortical layers were identified with CSD analysis by visual stimulation with full-field white flashes. The top of the initial current sink was considered to correspond to the upper edge of layer IV, and was used as a point of alignment for all recordings.

pairs ($F_{8,376} = 0.59$, $P = 0.79$). Thus, such time-averaged assessment of functional interaction by frequency band suggests that the alpha band is the key mediator of functional connectivity in the absence of visual input.

Motivated by this frequency-specific functional connectivity established by the correlation of slow fluctuations in alpha power (at the time-scale of seconds), we next computed magnitude square coherence ('coherence') to establish frequency-specific correlations between the LPI and V1 LFPs at a finer (millisecond) time-scale. The coherence values were normalized by subtracting the coherence for a matched, trial-shuffled dataset. Coherence showed a pronounced peak in the delta band and two smaller peaks in the alpha and gamma bands (Fig. 8A, coherence as a function of depth; Fig. 8B, depth-averaged coherence; Fig. 8C, coherence by frequency band). Two-way ANOVA showed that coherence was significantly

affected by LPI–V1 pairs ($F_{2,315} = 3.91$, $P = 0.02$). Coherence between LPI and the V1 supragranular layer was significantly stronger than coherence between LPI and V1 infragranular layers ($P < 0.05$). The main effect of frequency band was also significant ($F_{4,315} = 44.04$, $P < 0.001$). We found pronounced coherence in the delta band, moderate coherence in the alpha and theta bands, and weak coherence in the beta and gamma bands. There was no significant interaction between location and frequency band ($F_{8,315} = 0.23$, $P = 0.99$).

Functional connectivity by spike-phase coupling

Given the frequency-specific coupling between LPI and V1 at the spatial scale of LFP signals, we investigated whether functional connectivity spanning LFP and MUA measurements was also present.

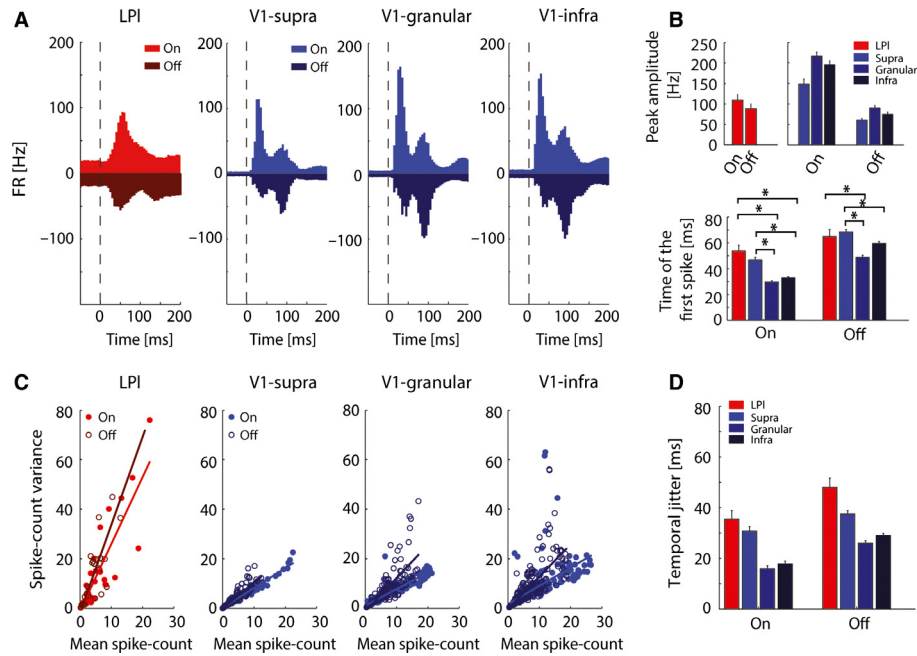


FIG. 6. Visual responses evoked by brief full-field stimulation. (A) Overall average PSTHs of MUA in LPI ($n = 28$) and the V1 cortical layers during visual stimulation (dashed line: stimulus onset): supragranular, layers 1–2/3, $n = 173$; granular, layer 4, $n = 151$; infragranular, layers 5–6, $n = 220$. (B) Top: mean peak response amplitude for LPI and the V1 layers during white ('on') and black ('off') flashes, measured from the PSTH. Bottom: mean time to first spike measured from stimulus onset to the first spike for LPI and the V1 layers. (C) Variance of the spike-counts as a function of the mean count. Variance increases with the mean, and a steeper slope was found for the LP–pulvinar complex than for the V1 layers. (D) Spike-timing (temporal) jitter of LPI ($n = 28$) and the V1 layers ($n = 173$, $n = 151$, and $n = 220$) for 'on' and 'off' responses. Temporal jitter was determined by calculating the standard deviation of the time of the first spike after stimulus onset. $*P < 0.05$. Error bars represent standard error of the mean. FR, firing rate.

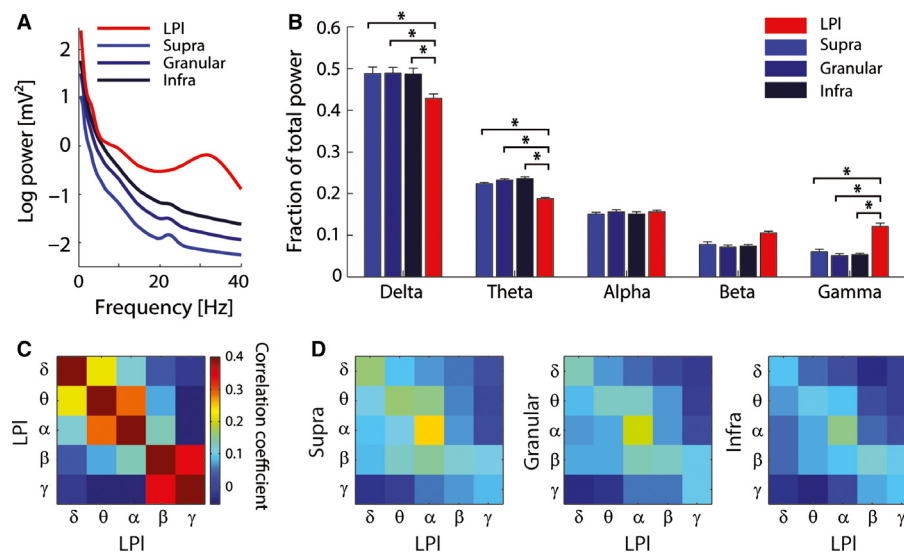


FIG. 7. LFP frequency structure in LPI and V1, and band-limited LFP power correlations during spontaneous activity. (A) Average LFP power spectra (red, LPI; blue, V1; shades indicate layers). (B) Power in each frequency band as a percentage of total power: delta, 0.5–4 Hz; theta, 4–8 Hz; alpha, 8–12 Hz; beta, 12–30 Hz; gamma, 30–40 Hz. $*P < 0.05$; error bars represent standard error of the mean. (C) Power autocorrelation for LPI. (D) Power correlation between LPI and the V1 layers.

Specifically, we investigated whether spikes in V1 showed a preferred LPI LFP phase and vice versa. We found strong and selective phase preference for V1 MUA in the delta band of the LPI LFP (Fig. 9A: top, spike-phase histograms; bottom, KL divergence as measure of non-uniformity of spike-phase distribution; delta, supra-granular, 95% CI 0.0023–0.0025; delta, granular, 95% CI 0.0070–0.0072; delta, infragranular, 95% CI 0.0150–0.0152). This coupling

in the delta band scaled with cortical depth, such that MUA in the infragranular layers showed the strongest phase preference. Given the anatomical projections from deep cortical layers to LPI (Fig. 3), the scaling of the spike preference with cortical depth may reflect the importance of cortico-thalamic projections in generating slow cortical oscillations. In the case of LPI MUA, we found that all frequency bands of the cortical LFP shaped the spike-timing of LPI

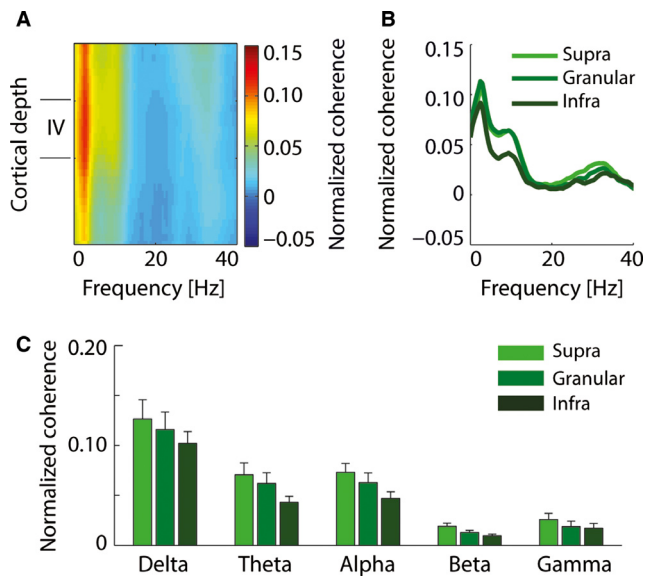


FIG. 8. Layer-dependent coherence between LP-pulvinar complex (LPI) and V1 during spontaneous activity. (A) Complete coherence depth profile (coherence as a function of V1 cortical depth). (B) Normalized coherence between LPI and different cortical layers. (C) Normalized coherence by frequency band and cortical layer. Error bars represent standard error of the mean.

MUA (Fig. 9B: LPI MUA as a function of V1 LFP phase). Consistently across frequency bands, such functional connectivity was strongest for supragranular layers (for example, in the delta frequency band: supragranular, 95% CI 0.0116–0.0119; granular, 95% CI 0.0081–0.0083; infragranular, 95% CI 0.0052–0.0053), in agreement with the anatomical projections of LPI to superficial cortical layers that we found in our tracing study. These data also agree with the power correlation and the LFP coherence analysis, which similarly showed stronger functional connectivity for the superficial layers. To confirm that the LFPs recorded in LPI and the V1 layers were not signals from neighbouring structures, we also computed spike-phase locking within each area (Fig. S3A). These results excluded the possibility that LFPs recorded in LPI are limited to volume transmission from the LGN or other nearby structures.

Network dynamics in response to synthetic and naturalistic visual input

Little is known about how LPI responds to dynamic, full-field visual stimulation. To fill this gap, we presented two types of 10-s visual stimuli (Fig. 10A): 1-Hz checkerboard frozen noise (NOI, ‘synthetic/artificial’) and a nature movie clip with foxes (FOX, ‘naturalistic’). Synthetic visual stimuli represent a key tool for the study of visual responses, but naturalistic visual input may engage different processing mechanisms (Simoncelli & Olshausen, 2001; Felsen & Dan, 2005). We compared MUA responses between the two stimuli in LPI and the V1 layers (Fig. 10B and C). MUA in LPI showed similar responses to NOI and FOX ($P > 0.05$, t -test). Using a two-way ANOVA with stimulus type and recording site as factors, we found that normalized MUA responses in the V1 layers were significantly affected by stimulus type (main effect of stimulus, $F_{1,102} = 10.1$, $P < 0.005$; no effect of recording site, $F_{2,102} = 0$, $P > 0.05$; no significant interaction, $F_{2,102} = 0$, $P > 0.05$), whereby V1 MUA was higher during naturalistic stimulation than during artificial stimulation (Fig. 10D).

To probe whether synthetic and naturalistic visual stimuli differentially modulated functional interactions between LPI and V1, we next examined the modulation of spike-phase locking between LPI and V1 at the level of LFPs and MUA (same analysis strategy as in Fig. 9). First, we quantified the LFP spectral characteristics of LPI and V1 before and during visual stimulation (Fig. 11). Similarly to the spectral structure during spontaneous activity (Fig. 7), power spectra before (REST) and during (NOI and FOX) visual stimulation showed pronounced power in the delta band (<4 Hz) in both LPI and V1 (all layers), and a clear spectral peak in the gamma band in LPI (~30 Hz).

Next, we probed for differential effects of synthetic and naturalistic visual stimulation on the spike-phase coupling between LPI and V1. We first examined V1 spikes and LPI LFP phase preferences during NOI and FOX visual stimulation in comparison with the phase preference during REST (Fig. 12). We found that the layer-specific phase preference for cortical MUA in the delta band of the LPI LFP was clearly modified during both NOI and FOX visual stimulation (Fig. 12A: KL divergence as measure of non-uniformity of spike phase during REST; delta, supragranular, 95% CI 0.0018–0.0021; delta, granular, 95% CI 0.0054–0.0060; delta, infragranular, 95% CI 0.0151–0.0158). During NOI stimulation, phase preferences were reduced in the infragranular layer, but increased in the supragranular layer, in the delta band (delta, supragranular, 95% CI 0.0090–0.0095; delta, granular, 95% CI 0.0052–0.0056; delta, infragranular, 95% CI 0.0099–0.0103). Meanwhile, phase preference in the other frequency bands was increased, with no distinct differences between layers. In contrast, during FOX visual stimulation, the layer-specific phase preference was only reduced in the delta band, and we observed no clear changes in the other frequency bands during FOX stimulation (delta, supragranular, 95% CI 0.0016–0.0019; delta, granular, 95% CI 0.0025–0.0027; delta, infragranular, 95% CI 0.0022–0.0023).

In the case of LPI MUA, we found that all frequency bands of the cortical LFP were coupled to the spike-timing of LPI MUAs during two types of visual stimuli, and that the strongest connectivity was still found in supragranular layers across frequency bands (Fig. 12B). Interestingly, the NOI stimulus and the FOX stimulus had opposite effects on the phase preference, whereby NOI increased phase preference and FOX reduced phase preference across all frequencies. Phase preference during the REST condition was comparable to that shown during spontaneous activity (Fig. 9). To examine the modulation of local spike-phase synchronization, we also computed spike-phase distributions for all frequency bands within each area during REST, NOI stimulation, and FOX stimulation (Fig. S3B). Similarly to cross-area phase preference, the NOI stimulus strengthened phase preference, whereas the FOX stimulus weakened phase preference. The phase preferences within LPI were not affected by visual stimuli. These data suggest that different visual stimuli not only caused different levels of MUA and LFP fluctuation, but also imposed different functional connectivity between LPI and V1.

Discussion

We characterized LPI and its layer-specific interaction dynamics with area 17 (V1) in ferrets, a model system with a relatively well-developed visual system including higher-order cortical visual areas (Law *et al.*, 1988; Manger *et al.*, 2002a,b, 2010; Patzke *et al.*, 2014). We found: (i) a histochemical substructure of the ferret LP–pulvinar complex (LPI) that is reciprocally connected with V1 in the ferret; (ii) that LPI robustly responded to full-field synthetic and

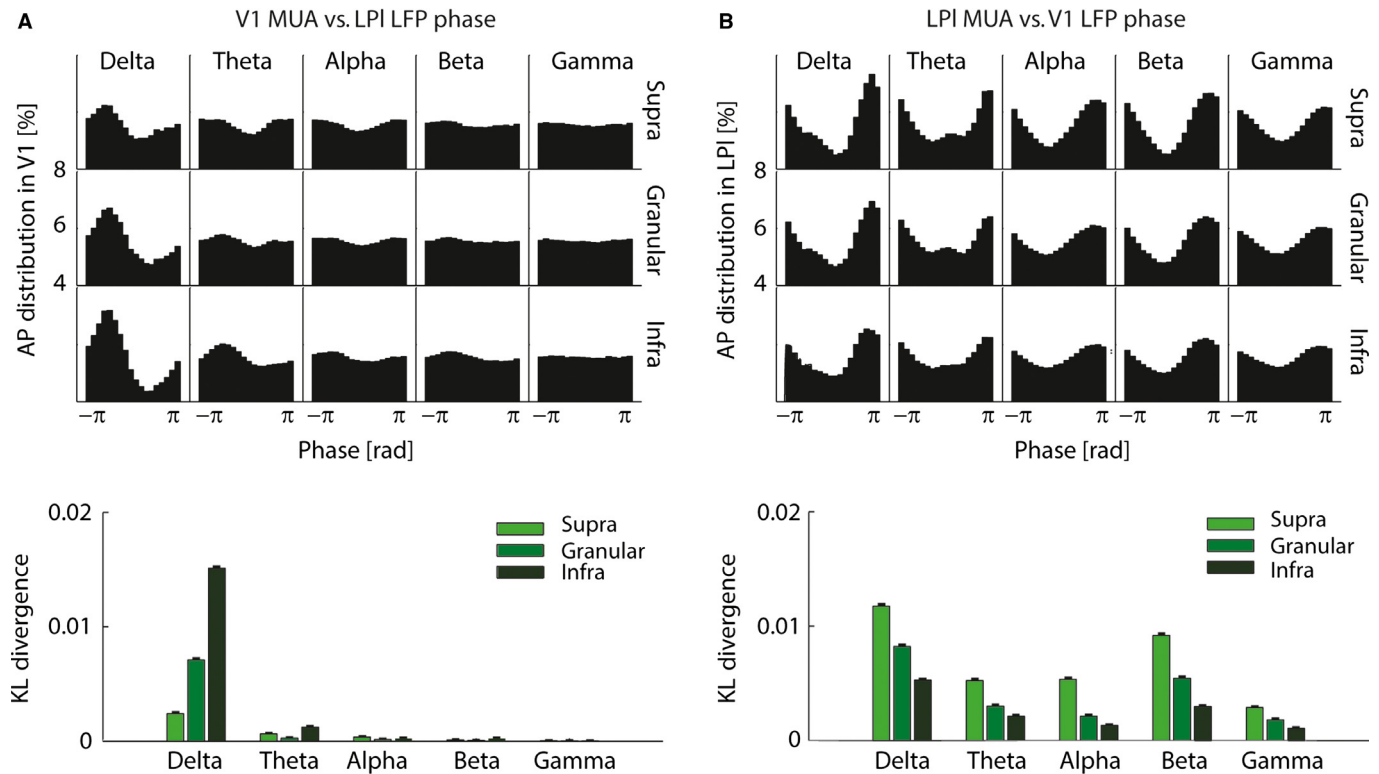


FIG. 9. Spike-phase coupling between LPI and the V1 cortical layers (spontaneous activity). (A) Top: preferred phase of firing of V1 MU spikes as a function of LPI LFP oscillation phase by cortical layer and frequency band. Bottom: KL divergence quantifies the degree of phase preference. Error bars denote 95% CIs determined by bootstrap. (B) Top: LPI MU spikes as a function of V1 LFP oscillation phase by cortical layer and frequency band. Bottom: KL divergence quantifies the degree of phase preference. Error bars as in A.

naturalistic visual input; (iii) frequency-specific and layer-specific functional connections between LPI and V1; and (iv) that the functional interactions between LPI and V1 were differentially modulated by different types of visual stimulation.

The visual thalamus consists of two main nuclei that project to the cortex. The LGN is a first-order thalamic nucleus that has been extensively studied in terms of its anatomical connectivity patterns, response properties, and strength of oscillatory activity (Jones, 2007; Saalman & Kastner, 2011). To our knowledge, the LP–pulvinar complex has not been previously studied in ferrets, so the comparison with other species provides important insights. However, there are discrepancies in nomenclature between the primate and the carnivore literature. The LP–pulvinar complex shows large variations between mammalian species, because the pulvinar nucleus has greatly increased in size and differentiation with progressive evolutionary development of the neocortex, whereas the opposite has occurred for the LP nucleus. The main subdivisions in the primate pulvinar nucleus are the lateral, medial and inferior pulvinar. In contrast, in the cat, seemingly similar structures have been referred to as subdivisions of the LP nucleus, with a fourth, poorly characterized nucleus referred to as the pulvinar nucleus (Jones, 2007). The pulvinar and LP nuclei are neighbouring structures, and, to some extent, resemble each other in histological appearance and connectivity; however, equivalent nuclei may not always have been recognized as such in different species [for a review, see Jones (2007)]. Inhomogeneous nomenclature is used for the subdivisions of the LP–pulvinar complex between species, and inconsistent naming is used by different authors for a given species. The LP–pulvinar complex of the ferret has been drawn in figures of several earlier studies

that focused on other brain areas (Herbert, 1963; Pallas *et al.*, 1990; Angelucci *et al.*, 1997; Manger *et al.*, 2002b; Highley *et al.*, 2003; Allman *et al.*, 2009; Manger *et al.*, 2010; Vazquez-Garcia *et al.*, 2014). However, the criteria used for subdivision schemes are either not explicitly provided or are unclear. In contrast, Jones (2007) describes the LP–pulvinar complex in the ferret thalamus in comparison with that of the cat based on sections stained for AChE and calcium-binding proteins. In our study, we followed Jones in terms of localization and terminology. On the basis of classic histochemical and immunohistochemical stains, we delineated LPI of the ferret as an intensely CO-stained and faintly AChE-stained subdivision of the caudo-lateral LP–pulvinar complex corresponding to that in the cat, a related carnivore. Besides structural features, each subdivision of the LP–pulvinar complex was also defined by a characteristic connectivity pattern. Here, we performed a tracing study, and showed a correspondence of the LPI connectivity pattern in the ferret with that in the cat. Specifically, we showed that LPI projects to area 17 and vice versa by using anterograde virus and retrograde tracer injections. Concerning the layer specificity of the projections from V1 to LPI, our results show involvement of layer V and VI cells, which differs from what is described in the cat (Abramson & Chalupa, 1985). These authors describe the cells projecting to LPI from area 17 and 18 as layer V pyramidal cells. Whether this mismatch is a species difference or is attributable to a different assessment of the location of the visual areas between authors cannot be determined from our data.

Our electrophysiological characterization of LPI revealed visually responsive MUA with late onset, and higher variability in terms of both spike-timing and overall spike-count (Fig. 6). Motivated by the

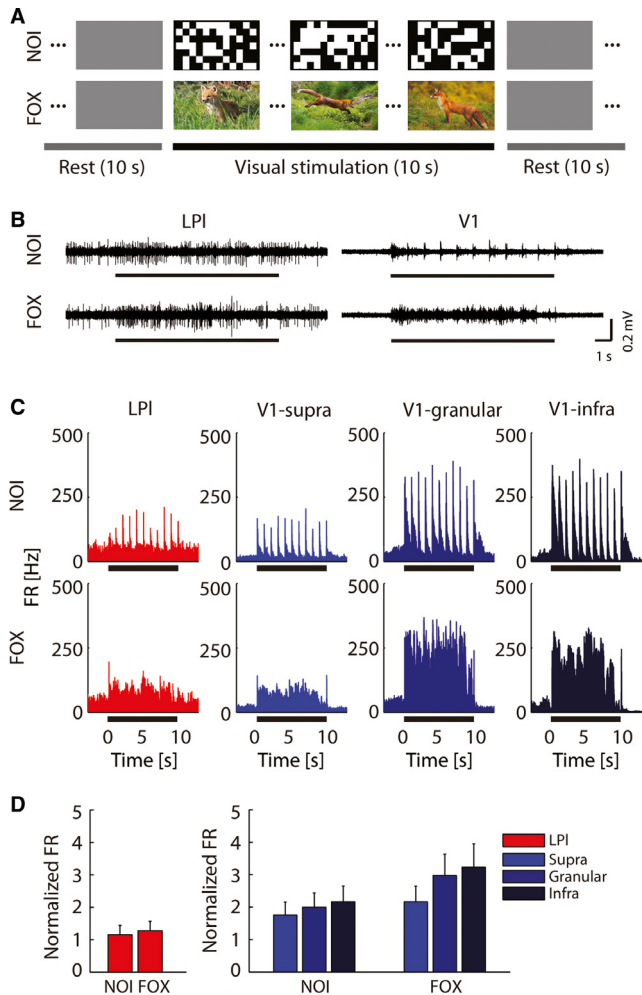


FIG. 10. Visual responses to synthetic and naturalistic stimuli. (A) Illustration of synthetic and naturalistic visual stimuli. Each trial consisted of 10 s of visual stimulation bracketed by 10 s of rest (grey screen). Each stimulus was presented 10 times, in a randomized order. (B) Representative high-pass-filtered raw traces indicate the modulation of LPI (left) and V1 (right) neuronal activity during NOI (top) and FOX (bottom) visual stimuli. Black lines indicate 10 s of stimulation. (C) PSTHs of representative MUA in LPI and the three layers of V1 in response to different types of visual stimuli. (D) Normalized firing rate (FR) of LPI and V1 MUA for different types of visual stimuli. Error bars represent standard error of the mean.

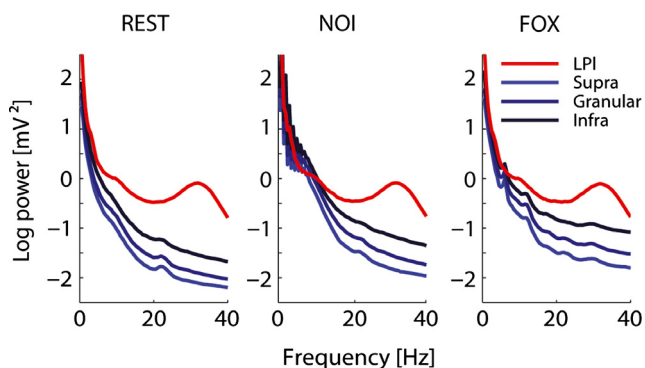


FIG. 11. LFP frequency structure in LPI and the V1 layers during visual stimulation: average LFP power spectra 10 s before (left) and during the NOI (middle) and FOX (right) stimuli (red, LPI; blue, V1; shades indicate layers).

demonstration of behaviourally important functional connectivity between the pulvinar area and visual cortices during cognitive tasks (Saalmann *et al.*, 2012), we investigated whether functional connectivity between LPI and V1 exists in the absence of behaviour, i.e. during anaesthesia characterized by complete loss of consciousness, and how it is altered by full-field visual input. To our knowledge, our study is the first demonstration of layer-specific functional connectivity between the LPI and V1. Importantly, our findings agree overall with what we predicted from our tracer injections and the canonical structural connectivity between cortical circuits and higher-order thalamic structures (Sherman, 2007). In essence, we found functional connectivity between LPI and both deep (infragranular) and superficial (supragranular) layers of V1. Three frequency bands stood out in our data: delta (<4 Hz), alpha (8–12 Hz), and gamma (>30 Hz). The prominence of activity in the delta band is probably the result of anaesthesia (Sellers *et al.*, 2015), although similar low-frequency orchestration of cortical network activity may occur in the awake, resting animal (Poulet & Petersen, 2008; Harris & Thiele, 2011). Second, functional interactions in the alpha band are in agreement with the canonical view that oscillations in the alpha band emerge from cortico-thalamic dynamics (da Silva *et al.*, 1973). Such coherence in the alpha band is consistent with the proposed role of the pulvinar nucleus in regulating cortical information flow during attentional states in the awake behaving primate (Saalmann *et al.*, 2012) and with the power fluctuations described for pulvinar and higher-order cortical areas in the resting state (Wang *et al.*, 2012). Third, we found interactions in the gamma band that may reflect a wider organization of network activity across areas by fast oscillations.

To further understand the functional interactions during visual processing, we presented synthetic and naturalistic visual stimuli while recording the neural activity from LPI and V1. Synthetic visual stimuli have a long history in vision neuroscience, as they elicit robust neuronal responses. However, visual circuits in the brain are assumed to be optimized for stimuli similar to the ones used during naturalistic visual stimulation (Simoncelli & Olshausen, 2001; Felsen & Dan, 2005). We found strong enhancement of low-frequency activity in V1 that reflected the temporal structure of the NOI stimulus. Interestingly, these differences were not observed in LPI. Furthermore, we found that spike-phase synchrony between V1 and LPI was increased during NOI stimulation (Fig. 12), which may imply that the response to the synthetic visual input predominated over endogenous interaction dynamics between V1 and LPI during the presentation of synthetic stimuli. In contrast, spike-phase coupling between these two areas was reduced during FOX stimulation (Fig. 12). This may reflect the fact that naturalistic stimuli show more complex spatio-temporal statistics that require more complex neuronal representation. We speculate that decreased macroscopic coupling, which implies higher entropy, facilitates the processing of naturalistic input.

Our recordings were performed under anaesthesia. In theory, neural information processing in the LP–pulvinar complex may be different in the awake animal, so the electrophysiological data presented here need to be interpreted with caution. Clearly, anaesthesia alters microscale and mesoscale network dynamics (Sellers *et al.*, 2013), but, at least at the level of global, resting state connectivity assayed by functional MRI, anaesthesia may not alter overall functional connectivity (Vincent *et al.*, 2007). Performing these experiments under anaesthesia enabled us to assay functional connectivity unperturbed by changes in overall brain state. Functional connectivity emerges at the intersection of the anatomical substrate (unaltered by anaesthesia) and the overall activity state (altered by

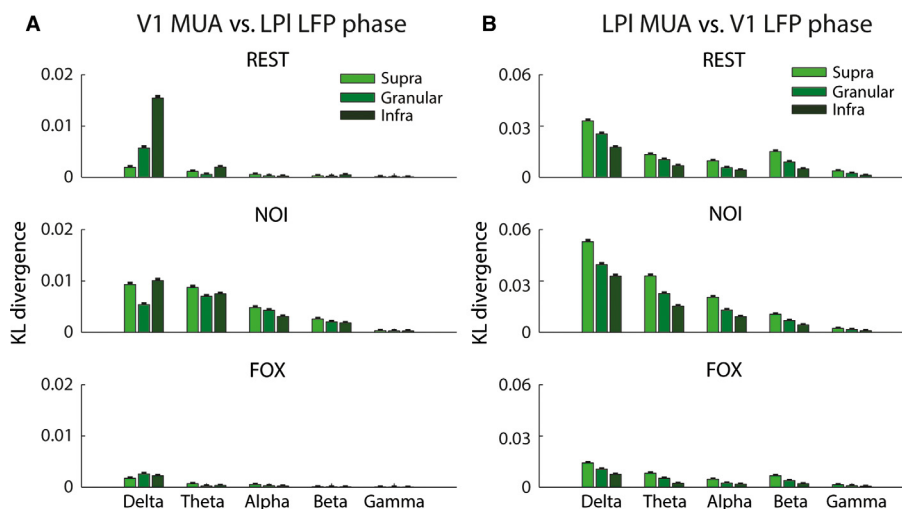


FIG. 12. Spike-phase coupling between LPI and the V1 cortical layers during visual stimulation (A) KL divergence quantifies the degree of phase preference of firing of V1 multiunit spikes as a function of LPI LFP oscillation phase by cortical layer and frequency band before (REST, top) and during NOI (middle) and FOX (bottom) stimulation. Error bars denote 95% CIs determined by bootstrap. (B) KL divergence quantifies the degree of phase preference of firing of LPI multiunit spikes as a function of V1 LFP oscillation phase by cortical layer and frequency band before (REST, top) and during NOI (middle) and FOX (bottom) stimulation. Error bars as in A.

anaesthesia). Indeed, our connectivity results are consistent with predictions based on the connections that we found in our anatomical studies and predictions based on the overall state of a fully anaesthetized animal (strong presence of delta oscillations). Nevertheless, further study of functional connectivity in the awake animal represents an important future direction.

The LP–pulvinar complex is a higher-order thalamic nucleus, and shows extensive bidirectional anatomical connections with the cortex. The functional role of these cortico-thalamo-cortical connections has remained mostly unclear. Two opposing conceptual frameworks for how higher-order thalamic nuclei and cortical areas interact have been proposed. The key dichotomy in these models boils down to the relative importance of cortico-cortical vs. cortico-pulvino-cortical connections for driving cortical areas. For example, in the visual system, area V2 receives input from both the pulvinar nucleus and from V1, with most of the afferents localizing in input layer 4 of V2 (Purushothaman *et al.*, 2012). A major debate is focused on the relative strength and functional relevance of these two inputs to V2 (Schiller & Malpeli, 1977; Felleman & Van Essen, 1991; Kaas & Lyon, 2007), and, more generally, on the question of whether the pulvinar nucleus acts as a driver or a modulator of visual areas (Sherman & Guillery, 2002; Theyel *et al.*, 2010; Sherman, 2012). Despite the fact that the defining physiological and molecular markers for drivers and modulators remain to be determined, it appears that pulvinar input to V2 resembles LGN–V1 connectivity, on the basis of VGlutT2 expression and greater synaptic bouton size, suggesting that the pulvinar nucleus is a driver of V2 (Marion *et al.*, 2013). In contrast to V2, it is commonly assumed that the LGN drives V1. The input from the pulvinar nucleus to V1 would therefore be, by definition, a modulatory input, but a recent study demonstrated a powerful effect of pharmacologically blocking the lateral pulvinar nucleus in terms of eliminating orientation tuning and visual responses in the superficial V1 in a primate model (Purushothaman *et al.*, 2012).

It is therefore worthwhile comparing our electrophysiological results with the known anatomical connections of V1 with the pulvinar nucleus in other species. Specifically, layer 5B of V1 connects to the pulvinar nucleus (Lund *et al.*, 1975; Ogren & Hendrickson,

1977), and projections from the pulvinar nucleus to V1 target layers 1 and 2 (Benevento & Rezak, 1976) in the primate. We hypothesized that these anatomical connections constrain the functional connectivity between the pulvinar nucleus and V1. Indeed, our findings agree overall with what is predicted from the canonical structural connectivity between cortical circuits and higher-order thalamic structures (Sherman, 2007). In this model, layer 5 of a primary sensory cortex drives higher-order thalamic nuclei such as the pulvinar nucleus. In turn, the higher-order nucleus provides projections back to layer 1 of V1. However, our electrophysiological recordings do not allow the resolution of individual supragranular and infragranular layers. In essence, we found functional connectivity between LPI and both the deep (infragranular) and the superficial (supragranular) layers of V1. Although our results do not provide a definite answer to the question of whether the LP–pulvinar complex is a driver or modulator of V1, the presence of layer-specific functional connections between the two brain areas supports the importance of this connection for neural processing, even in the absence of visual input.

To our knowledge, the data presented here represent the first description of the functional network interactions between the LP–pulvinar complex and V1 in any species. Elucidating functional connectivity has evolved into a key approach for understanding both how physiological and pathological states emerge in complex, interconnected networks (Rubinov & Sporns, 2010). Specific interaction dynamics as found here probably represent the fundamental mechanism by which information is selectively routed in brain networks. Our study describes several specific functional connections between the LP–pulvinar complex and V1. Combining microscopic and mesoscopic electrophysiological assays with high temporal precision enabled us to provide this novel map of functional connectivity in this cortico-thalamo-cortical circuit. Interestingly, changes to the morphology and function of the pulvinar nucleus have been associated with a number of neurological and psychiatric disorders (Karnath *et al.*, 2002; Highley *et al.*, 2003; Baldauf *et al.*, 2005; Andrews *et al.*, 2006; Rosenberg *et al.*, 2006; Burlina *et al.*, 2008; Kim *et al.*, 2008; Coscia *et al.*, 2009; Cronenwett & Csernansky, 2010; Li *et al.*, 2012). It remains to be seen how impairment of cor-

tico-thalamo-cortical loops contributes to these disease processes, possibly as a substrate of thalamo-cortical ‘dysrhythmias’ (Llinas *et al.*, 1999).

Author contributions

C. Yu, K. K. Sellers, R. Murrow and F. Fröhlich designed the experiments. C. Yu and K. K. Sellers performed the experiments. Y.-Y. I. Shih performed the MRI study. C. Yu, S. Radtke-Schuller, J. Lu, Y. Li and F. Fröhlich analysed the data. C. Yu, L. Xing and V. Ghukasyan performed the confocal imaging. C. Yu, K. K. Sellers, S. Radtke-Schuller, R. Murrow and F. Fröhlich wrote the manuscript.

Conflicts of interest

The authors declare no competing financial interests.

Supporting Information

Additional supporting information can be found in the online version of this article:

Fig. S1. Anatomy of ferret LP–pulvinar complex.

Fig. S2. Identification of recording sites.

Fig. S3. Local spike–phase distribution in LP1 and V1 during spontaneous activity and during visual stimulation.

Table S1. Anatomical coordinates of responsive and non-responsive recording sites.

Acknowledgements

The authors thank the members of the Fröhlich Laboratory for their support, in particular Stephen Schmidt for his programming expertise, and the laboratory of Dr Casagrande at Vanderbilt University for assistance with histochemical protocols. The authors appreciate the helpful input to an earlier version of the manuscript by Dr Ehud Ahissar. The authors gratefully acknowledge the funding sources; the work was funded, in part, by a donation from Dean and Brenda Proctor and in part by the National Institute of Mental Health of the National Institutes of Health under Award Number R01MH101547. The content is solely the responsibility of the authors, and does not necessarily represent the official views of the National Institutes of Health. Imaging was supported by the Confocal and Multiphoton Imaging Core of NINDS Center Grant P30 NS045892.

Abbreviations

AChE, acetylcholinesterase; CI, confidence interval; CO, cytochrome oxidase; CSD, current source density; CTB, cholera toxin subunit B; DAPI, 4',6-diamidino-2-phenylindole; KL, Kullback–Leibler; LFP, local field potential; LGN, lateral geniculate nucleus; LP, lateral posterior; LP1, lateral part of the lateral posterior nucleus of the lateral posterior–pulvinar complex; MRI, magnetic resonance imaging; MUA, multiunit activity; V1, primary visual cortex; VGluT2, vesicular glutamate transporter 2.

References

Abramson, B.P. & Chalupa, L.M. (1985) The laminar distribution of cortical connections with the tecto- and cortico-recipient zones in the cat's lateral posterior nucleus. *Neuroscience*, **15**, 81–95.

Allman, B.L., Keniston, L.P. & Meredith, M.A. (2009) Adult deafness induces somatosensory conversion of ferret auditory cortex. *Proc. Natl. Acad. Sci. USA*, **106**, 5925–5930.

Andrews, J., Wang, L., Csernansky, J.G., Gado, M.H. & Barch, D.M. (2006) Abnormalities of thalamic activation and cognition in schizophrenia. *Am. J. Psychiat.*, **163**, 463–469.

Angelucci, A., Clasca, F., Bricolo, E., Cramer, K.S. & Sur, M. (1997) Experimentally induced retinal projections to the ferret auditory thalamus: devel-

opment of clustered eye-specific patterns in a novel target. *J. Neurosci.*, **17**, 2040–2055.

Arend, I., Rafal, R. & Ward, R. (2008) Spatial and temporal deficits are regionally dissociable in patients with pulvinar lesions. *Brain*, **131**, 2140–2152.

Baldauf, Z.B., Chomsung, R.D., Carden, W.B., May, P.J. & Bickford, M.E. (2005) Ultrastructural analysis of projections to the pulvinar nucleus of the cat. I: middle suprasylvian gyrus (areas 5 and 7). *J. Comp. Neurol.*, **485**, 87–107.

Benevento, L.A. & Rezak, M. (1976) The cortical projections of the inferior pulvinar and adjacent lateral pulvinar in the rhesus monkey (*Macaca mulatta*): an autoradiographic study. *Brain Res.*, **108**, 1–24.

Berson, D.M. & Graybiel, A.M. (1978) Parallel thalamic zones in the LP–pulvinar complex of the cat identified by their afferent and efferent connections. *Brain Res.*, **147**, 139–148.

Berson, D.M. & Graybiel, A.M. (1983) Organization of the striate-recipient zone of the cat lateralis posterior–pulvinar complex and its relations with the geniculostriate system. *Neuroscience*, **9**, 337–372.

Brainard, D.H. (1997) The psychophysics toolbox. *Spat. Vis.*, **10**, 433–436.

Burlina, A.P., Manara, R., Caillaud, C., Laissy, J.-P., Severino, M., Klein, I., Burlina, A. & Lidove, O. (2008) The pulvinar sign: frequency and clinical correlations in Fabry disease. *J. Neurol.*, **255**, 738–744.

Buschman, T.J. & Miller, E.K. (2007) Top-down versus bottom-up control of attention in the prefrontal and posterior parietal cortices. *Science*, **315**, 1860–1862.

Chalupa, L.M. (1977) A review of cat and monkey studies implicating the pulvinar in visual function. *Behav. Biol.*, **20**, 149–167.

Coscia, D.M., Narr, K.L., Robinson, D.G., Hamilton, L.S., Sevy, S., Burdick, K.E., Gunduz-Bruce, H., McCormack, J., Bilder, R.M. & Szeszko, P.R. (2009) Volumetric and shape analysis of the thalamus in first-episode schizophrenia. *Hum. Brain Mapp.*, **30**, 1236–1245.

Cronenwett, W.J. & Csernansky, J. (2010) Thalamic pathology in schizophrenia. *Curr. Top. Behav. Neurosci.*, **4**, 509–528.

Felleman, D.J. & Van Essen, D.C. (1991) Distributed hierarchical processing in the primate cerebral cortex. *Cereb. Cortex*, **1**, 1–47.

Felsen, G. & Dan, Y. (2005) A natural approach to studying vision. *Nat. Neurosci.*, **8**, 1643–1646.

Fischer, J. & Whitney, D. (2012) Attention gates visual coding in the human pulvinar. *Nat. Commun.*, **3**, 1051.

Fröhlich, F. & McCormick, D.A. (2010) Endogenous electric fields may guide neocortical network activity. *Neuron*, **67**, 129–143.

Gallyas, F. (1979) Simultaneous determination of the amounts of metallic and ‘reducible’ silver in histologic specimens. *Histochemistry*, **64**, 77–86.

Geneser-Jensen, F.A. & Blackstad, T.W. (1971) Distribution of acetyl cholinesterase in the hippocampal region of the guinea pig. I. Entorhinal area, parasubiculum, and presubiculum. *Z. Zellforsch. Mik. Ana.*, **114**, 460–481.

Gregoriou, G.G., Gotts, S.J., Zhou, H. & Desimone, R. (2009) High-frequency, long-range coupling between prefrontal and visual cortex during attention. *Science*, **324**, 1207–1210.

Grieve, K.L., Acuña, C. & Cudeiro, J. (2000) The primate pulvinar nuclei: vision and action. *Trends Neurosci.*, **23**, 35–39.

Harris, K.D. & Thiele, A. (2011) Cortical state and attention. *Nat. Rev. Neurosci.*, **12**, 509–523.

Herbert, J. (1963) Nuclear structure of the thalamus of the ferret. *J. Comp. Neurol.*, **120**, 105–127.

Highley, J.R., Walker, M.A., Crow, T.J., Esiri, M.M. & Harrison, P.J. (2003) Low medial and lateral right pulvinar volumes in schizophrenia: a post-mortem study. *Am. J. Psychiat.*, **160**, 1177–1179.

Jones, E.G. (2007) *The Thalamus*. Cambridge University Press, Cambridge, New York.

Kaas, J.H. & Lyon, D.C. (2007) Pulvinar contributions to the dorsal and ventral streams of visual processing in primates. *Brain Res. Rev.*, **55**, 285–296.

Karnath, H.O., Himmelbach, M. & Rorden, C. (2002) The subcortical anatomy of human spatial neglect: putamen, caudate nucleus and pulvinar. *Brain*, **125**, 350–360.

Kastner, S., O'Connor, D.H., Fukui, M.M., Fehd, H.M., Herwig, U. & Pinsk, M.A. (2004) Functional imaging of the human lateral geniculate nucleus and pulvinar. *J. Neurophysiol.*, **91**, 438–448.

Kim, D.-J., Kim, J.-J., Park, J.-Y., Lee, S.-Y., Kim, J., Kim, I.-Y., Kim, S.I. & Park, H.-J. (2008) Quantification of thalamocortical tracts in schizophrenia on probabilistic maps. *NeuroReport*, **19**, 399–403.

Kohn, D.F. (1997) *Anesthesia and Analgesia in Laboratory Animals*. Academic Press, San Diego, CA.

Law, M.I., Zahs, K.R. & Stryker, M.P. (1988) Organization of primary visual cortex (area 17) in the ferret. *J. Comp. Neurol.*, **278**, 157–180.

- Li, X., Sroubek, A., Kelly, M.S., Lesser, I., Sussman, E., He, Y., Branch, C. & Foxe, J.J. (2012) Atypical pulvinar–cortical pathways during sustained attention performance in children with attention-deficit/hyperactivity disorder. *J. Am. Acad. Child Psy.*, **51**, 1197–1207.
- Linias, R.R., Ribary, U., Jeanmonod, D., Kronberg, E. & Mitra, P.P. (1999) Thalamocortical dysrhythmia: a neurological and neuropsychiatric syndrome characterized by magnetoencephalography. *Proc. Natl. Acad. Sci. USA*, **96**, 15222–15227.
- Lund, J.S., Lund, R.D., Hendrickson, A.E., Bunt, A.H. & Fuchs, A.F. (1975) The origin of efferent pathways from the primary visual cortex, area 17, of the macaque monkey as shown by retrograde transport of horseradish peroxidase. *J. Comp. Neurol.*, **164**, 287–303.
- Manger, P.R., Kiper, D., Masiello, I., Murillo, L., Tettoni, L., Hunyadi, Z. & Innocenti, G.M. (2002a) The representation of the visual field in three extrastriate areas of the ferret (*Mustela putorius*) and the relationship of retinotopy and field boundaries to callosal connectivity. *Cereb. Cortex*, **12**, 423–437.
- Manger, P.R., Masiello, I. & Innocenti, G.M. (2002b) Areal organization of the posterior parietal cortex of the ferret (*Mustela putorius*). *Cereb. Cortex*, **12**, 1280–1297.
- Manger, P.R., Restrepo, C.E. & Innocenti, G.M. (2010) The superior colliculus of the ferret: cortical afferents and efferent connections to dorsal thalamus. *Brain Res.*, **1353**, 74–85.
- Marion, R., Li, K., Purushothaman, G., Jiang, Y. & Casagrande, V.A. (2013) Morphological and neurochemical comparisons between pulvinar and V1 projections to V2. *J. Comp. Neurol.*, **521**, 813–832.
- Ogren, M.P. & Hendrickson, A.E. (1977) The distribution of pulvinar terminals in visual areas 17 and 18 of the monkey. *Brain Res.*, **137**, 343–350.
- Pallas, S.L., Roe, A.W. & Sur, M. (1990) Visual projections induced into the auditory pathway of ferrets. I. Novel inputs to primary auditory cortex (AI) from the LP/pulvinar complex and the topography of the MGN-AI projection. *J. Comp. Neurol.*, **298**, 50–68.
- Patzke, N., Innocenti, G.M. & Manger, P.R. (2014) The claustrum of the ferret: afferent and efferent connections to lower and higher order visual cortical areas. *Front. Syst. Neurosci.*, **8**, 31.
- Petersen, K.H., Hagen, E. & Einevoll, G.T. (2008) Estimation of population firing rates and current source densities from laminar electrode recordings. *J. Comp. Neurosci.*, **24**, 291–313.
- Poulet, J.F. & Petersen, C.C. (2008) Internal brain state regulates membrane potential synchrony in barrel cortex of behaving mice. *Nature*, **454**, 881–885.
- Purushothaman, G., Marion, R., Li, K. & Casagrande, V.A. (2012) Gating and control of primary visual cortex by pulvinar. *Nat. Neurosci.*, **15**, 905–912.
- Raczkowski, D. & Rosenquist, A.C. (1983) Connections of the multiple visual cortical areas with the lateral posterior–pulvinar complex and adjacent thalamic nuclei in the cat. *J. Neurosci.*, **3**, 1912–1942.
- Rappelsberger, P., Pockberger, H. & Petsche, H. (1981) Current source density analysis: methods and application to simultaneously recorded field potentials of the rabbit's visual cortex. *Pflug. Arch.*, **389**, 159–170.
- Rinne, P., Hassan, M., Goniotakis, D., Chohan, K., Sharma, P., Langdon, D., Soto, D. & Bentley, P. (2013) Triple dissociation of attention networks in stroke according to lesion location. *Neurology*, **81**, 812–820.
- Rosenberg, D.S., Mauguière, F., Demarquay, G., Ryvlin, P., Isnard, J., Fischer, C., Guénot, M. & Magnin, M. (2006) Involvement of medial pulvinar thalamic nucleus in human temporal lobe seizures. *Epilepsia*, **47**, 98–107.
- Rubinov, M. & Sporns, O. (2010) Complex network measures of brain connectivity: uses and interpretations. *NeuroImage*, **52**, 1059–1069.
- Saalmann, Y.B. & Kastner, S. (2011) Cognitive and perceptual functions of the visual thalamus. *Neuron*, **71**, 209–223.
- Saalmann, Y.B., Pinsk, M.A., Wang, L., Li, X. & Kastner, S. (2012) The pulvinar regulates information transmission between cortical areas based on attention demands. *Science*, **337**, 753–756.
- Schiller, P.H. & Malpel, J.G. (1977) The effect of striate cortex cooling on area 18 cells in the monkey. *Brain Res.*, **126**, 366–369.
- Segraves, M.A. & Rosenquist, A.C. (1982) The afferent and efferent callosal connections of retinotopically defined areas in cat cortex. *J. Neurosci.*, **2**, 1090–1107.
- Sellers, K.K., Bennett, D.V., Hutt, A. & Frohlich, F. (2013) Anesthesia differentially modulates spontaneous network dynamics by cortical area and layer. *J. Neurophysiol.*, **110**, 2739–2751.
- Sellers, K.K., Bennett, D.V., Hutt, A., Williams, J.H. & Frohlich, F. (2015) Awake versus anesthetized: layer-specific sensory processing in visual cortex and functional connectivity between cortical areas. *J. Neurophysiol.*, **113**, 3798–3815.
- Sherman, S.M. (2007) The thalamus is more than just a relay. *Curr. Opin. Neurobiol.*, **17**, 417–422.
- Sherman, S.M. (2012) Thalamocortical interactions. *Curr. Opin. Neurobiol.*, **22**, 575–579.
- Sherman, S.M. & Guillery, R.W. (2002) The role of the thalamus in the flow of information to the cortex. *Philos. T Roy Soc. B.*, **357**, 1695–1708.
- da Silva, F.H., van Lierop, T.H., Schrijer, C.F. & van Leeuwen, W.S. (1973) Organization of thalamic and cortical alpha rhythms: spectra and coherences. *Electroen. Clin. Neuro.*, **35**, 627–639.
- Simoncelli, E.P. & Olshausen, B.A. (2001) Natural image statistics and neural representation. *Annu. Rev. Neurosci.*, **24**, 1193–1216.
- Snow, J.C., Allen, H.A., Rafal, R.D. & Humphreys, G.W. (2009) Impaired attentional selection following lesions to human pulvinar: evidence for homology between human and monkey. *Proc. Natl. Acad. Sci. USA*, **106**, 4054–4059.
- Theyel, B.B., Llano, D.A. & Sherman, S.M. (2010) The corticothalamocortical circuit drives higher-order cortex in the mouse. *Nat. Neurosci.*, **13**, 84–88.
- Ulbert, I., Halgren, E., Heit, G. & Karmos, G. (2001) Multiple microelectrode-recording system for human intracortical applications. *J. Neurosci. Meth.*, **106**, 69–79.
- Updyke, B.V. (1981) Projections from visual areas of the middle suprasylvian sulcus onto the lateral posterior complex and adjacent thalamic nuclei in cat. *J. Comp. Neurol.*, **201**, 477–506.
- Vazquez-Garcia, M., Wallman, M.J. & Timofeev, I. (2014) Somatotopic organization of ferret thalamus. *Front. Integr. Neurosci.*, **8**, 90.
- Vincent, J.L., Patel, G.H., Fox, M.D., Snyder, A.Z., Baker, J.T., Van Essen, D.C., Zempel, J.M., Snyder, L.H., Corbetta, M. & Raichle, M.E. (2007) Intrinsic functional architecture in the anaesthetized monkey brain. *Nature*, **447**, 83–86.
- Wang, L., Saalmann, Y.B., Pinsk, M.A., Arcaro, M.J. & Kastner, S. (2012) Electrophysiological low-frequency coherence and cross-frequency coupling contribute to BOLD connectivity. *Neuron*, **76**, 1010–1020.
- Wiser, A.K. & Callaway, E.M. (1996) Contributions of individual layer 6 pyramidal neurons to local circuitry in macaque primary visual cortex. *J. Neurosci.*, **16**, 2724–2739.
- Wong-Riley, M. (1979) Changes in the visual system of monocularly sutured or enucleated cats demonstrable with cytochrome oxidase histochemistry. *Brain Res.*, **171**, 11–28.
- Zhang, J., Chu, K.-W., Teague, E.B., Newmark, R.E. & Buchsbaum, M.S. (2013) fMRI assessment of thalamocortical connectivity during attentional performance. *Magn. Reson. Imaging*, **31**, 1112–1118.